CMIP6 Models Overestimate the North Atlantic Eddy-Driven Jet Persistence

Albert Ossó[1] and Florian Ennemoser[1]

[1]Wegener Center for Climate and Global Change, University of Graz

April 19, 2024

Abstract

Persistent fluctuations in the latitudinal position of the North Atlantic (NATL) jet stream are associated with extreme weather anomalies, particularly over Europe. Therefore, it is crucial to understand how the jet stream persistence might change in response to increased greenhouse gases to deliver useful regional climate projections. This study examines the persistence of the North Atlantic jet stream latitudinal fluctuations in CMIP6 and ERA5. We found that CMIP6 models consistently overestimate the persistence compared to ERA5 during the historical period. This discrepancy appears linked to too weak transient eddies over the NATL in CMIP6 models.

By the end of the XXI century, CMIP6 models forced with the SSP585 scenario project a reduction of the jet fluctuations persistence of about 10% during the summer season. The evidence suggests this reduction is linked to a slower NATL jet during the summer months.

Hosted file

`A.OSSO_GRL_review_notrackChanges.docx` available at https://authorea.com/users/714669/articles/848370-cmip6-models-overestimate-the-north-atlantic-eddy-driven-jet-persistence

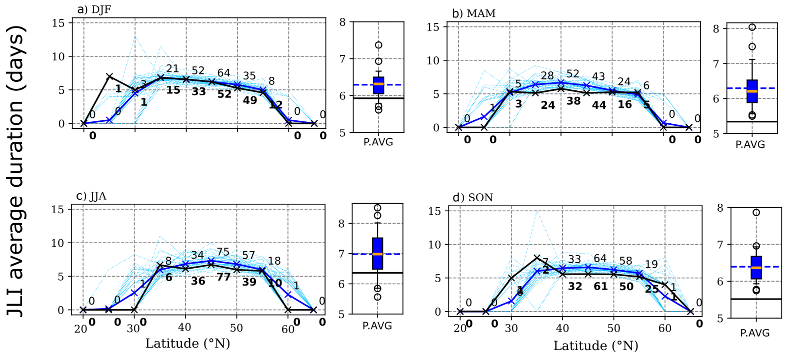
JLI average duration (days)
a) DJF
b) MAM
c) JJA
d) SON
P.AVG
Latitude (°N)

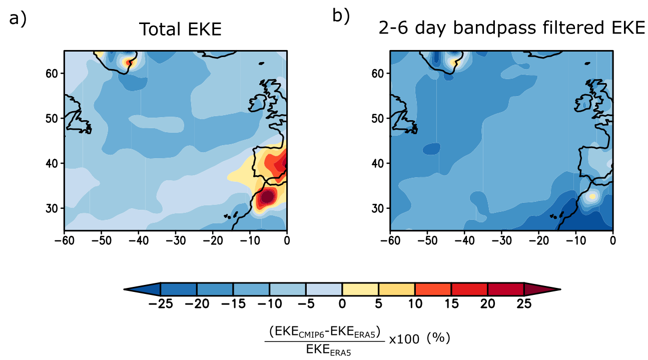

a)
Total EKE
b)
2-6 day bandpass filtered EKE
60
50
40
30
−60 −50 −40 −30 −20 −10 0
−25 −20 −15 −10 −5 0 5 10 15 20 25
(EKE_CMIP6-EKE_ERA5) / EKE_ERA5 x100 (%)

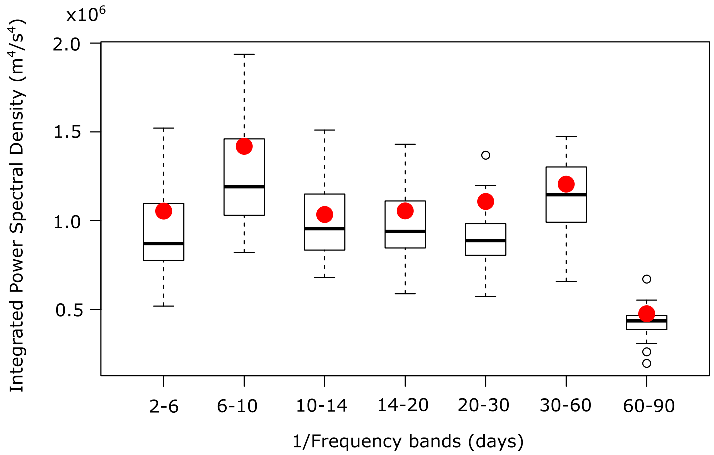
x10^6
2.0
1.5
1.0
0.5
Integrated Power Spectral Density (m^4/s^4)
2-6
6-10
10-14
14-20
20-30
30-60
60-90
1/Frequency bands (days)

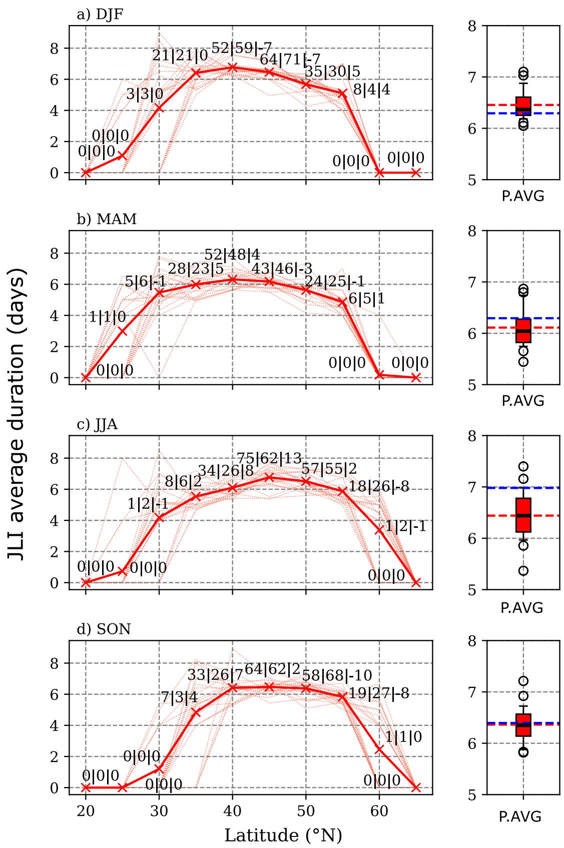
a) DJF
b) MAM
c) JJA
d) SON
JLI average duration (days)
Latitude (°N)
P.AVG
0|0|0
0|0|0
3|3|0
21|21|0
52|59|-7
64|71|-7
35|30|5
8|4|4
0|0|0
0|0|0
1|1|0
0|0|0
5|6|-1
28|23|5
52|48|4
43|46|-3
24|25|-1
6|5|1
0|0|0
0|0|0
0|0|0
0|0|0
1|2|-1
8|6|2
34|26|8
75|62|13
57|55|2
18|26|-8
1|2|-1
0|0|0
0|0|0
0|0|0
0|0|0
7|3|4
33|26|7
64|62|2
58|68|-10
19|27|-8
1|1|0
0|0|0

Manuscript submitted to Geophysical Research Letters

CMIP6 Models Overestimate the North Atlantic Eddy-Driven Jet Persistence

Albert Ossó[1] and Florian Ennemoser[1]

[1] Wegener Center for Climate and Global Change, University of Graz, Graz, Austria

Corresponding author: Albert Ossó (albert.osso-castillon@uni-graz.at)

Key Points:

- CMIP6 models overestimate the persistence of the latitudinal fluctuations of the eddy-driven jet stream over the North Atlantic.
- The overestimation of the jet persistence in CMIP6 is likely due to too weak transient eddies over the North Atlantic storm track.
- By the end of the XXI century, CMIP6 models forced with increasing greenhouse gases project a decrease of jet persistence in summer.

Abstract

Persistent fluctuations in the latitudinal position of the North Atlantic (NATL) jet stream are associated with extreme weather anomalies, particularly over Europe. Therefore, it is crucial to understand how the jet stream persistence might change in response to increased greenhouse gases to deliver useful regional climate projections. This study examines the persistence of the North Atlantic jet stream latitudinal fluctuations in CMIP6 and ERA5. We found that CMIP6 models consistently overestimate the persistence compared to ERA5 during the historical period. This discrepancy appears linked to too weak transient eddies over the NATL in CMIP6 models.

By the end of the XXI century, CMIP6 models forced with the SSP585 scenario project a reduction of the jet fluctuations persistence of about 10% during the summer season. The evidence suggests this reduction is linked to a slower NATL jet during the summer months.

Plain Language Summary

The NATL jet stream is key in determining the weather and climate over the NATL and European regions. The jet continuously fluctuates in latitude and strength and guides the storms along its path. A particular situation arises when these fluctuations become anomalously persistent and lock particular hydroclimate regimes in place for longer than usual. This situation can lead to extreme events such as drought or flooding. In this study, we investigate how CMIP6 models simulate the NATL jet stream latitudinal fluctuations and compare it with the ERA5 reanalysis dataset. We found that the models systematically overestimate the persistence of these fluctuations. We show that the overestimation is likely due to too weak transient eddies in the models over the NATL storm track. Overall, this study highlights the importance of understanding the origin of these biases and investigating how they might impact the projections of persistent events, especially extreme events. Improving the model representation of the atmospheric circulation persistence is crucial to reducing and constraining the uncertainty in regional climate change projections.

1. Introduction

Observational evidence indicates that extreme rainfall and heat events have become more frequent, intense and persistent during summer and winter since the latter half of the 20th century (e.g., Fischer and Knutti, 2015; Pfleiderer & Coumou, 2018). Some of the drivers of these changes have been linked to direct radiative forcing and thermodynamic feedback mechanisms associated with increased greenhouse gases (GHG) concentration (e.g., Coumou et al., 2012). However, the extent of these changes cannot be explained as a response to thermodynamic forcing alone, suggesting that changes in the atmospheric circulation must also play an important role.

One critical factor amplifying the potential for an atmospheric anomaly to lead to high-impact weather and climate events is their persistence. For instance, persistent shifts in the jet stream and storm tracks (e.g., 2007 UK floods; Blackburn et al., 2008), persistent blocking highs (e.g., 2003 European heatwave, 2010 Russian heatwave), or persistent stationary wave patterns (e.g., Kornhuber et al., 2017). In a recent study, Galfi and Messori (2023) analyzed a 1000-year-long pre-industrial control simulation of the MPI-ESM-LR and found that long-lasting anomalies in the NATL jet latitude position, speed and zonality are associated with more frequent and persistent episodes of extreme temperatures and precipitation across Europe during winter.

Over recent decades, numerous studies have suggested that weakened meridional temperature gradients in the Northern Hemisphere (hereafter, NH) due to Arctic Amplification (hereafter, AA) have led to deceleration of the westerly winds (Coumou et al., 2015; Vavrus et al., 2017), increased north-south jet meandering (Cattiaux et al., 2016; Di Capua & Coumou, 2016; Vavrus et al., 2017) and more persistent and amplified wave-like anomalies at mid-latitudes (Francis et al., 2018; 2020). However, the significance and causal relation of these trends with AA has been shown to depend on the methodologies employed (Hoskins & Woollings, 2015; Blackport & Screen, 2020), and modelling evidence remains inconclusive (Hassanzadeh et al., 2014; Smith et al., 2022).

A few studies have examined projected changes in persistence. For instance, Li and Thompson (2021) identified a robust, globally widespread change in surface temperature persistence by the end of the 21st century in four large model ensembles. They suggest that changes in persistence are driven by multiple mechanisms with strong regional variations. Other research has focused on projected changes in atmospheric blocking, indicating an overall reduction in its frequency across the NH (Masato et al., 2013; Matsueda et al., 2009). This blocking reduction has been partly linked to the projected poleward shift of the jet stream (Hoskins & Woollings, 2015).

Understanding the dynamics governing persistent weather events is an area of intensive research. It is crucial to evaluate the accuracy of climate models in capturing this persistence for reliable long-term projections, especially regarding high-impact weather phenomena (e.g., Tuel and Martius, 2023). In particular, studies have consistently highlighted the strong association between latitudinal shifts in the jet stream and extreme weather occurrences over Europe (Galfi & Messori, 2023; Mahlstein et al., 2012; Cattiaux et al., 2010; Trigo et al., 2013). Hence, it is imperative for models to capture these dynamics accurately.

In this manuscript, we critically evaluate the persistence of the NATL eddy-driven jet stream latitudinal fluctuations in CMIP6 models while investigating the underlying causes of model biases. Additionally, we examine projected changes in jet stream persistence by the end of the 21st century.

2. Data and Methodology

Datasets

We analyze daily zonal and meridional wind at 700hPa and precipitation from 35 models from the CMIP6 ensemble for the 1980-2014 period (hereafter, we will refer to this period as HIST), forced with the CMIP6 recommended historical forcing (Eyring et al., 2016). The r1i1p1f1 member of each model is used. Additionally, we use reanalysis data from the ERA5 reanalysis data from the European Centre for Medium-Range Weather Forecasts (ECMWF) (Hersbach et al., 2020).

We also use CMIP6 models forced with the projected emission of the future scenario of shared socioeconomic pathway 5 RCP8.5 (SSP585) to analyze future changes in persistence as it likely poses the highest signal against HIST (O'Neill et al., 2014). The last 35 years (2065 to 2099) from this scenario are taken as the future reference period (hereafter, we will refer to this period as FUT). Here, 22 models that intersect with HIST are analyzed.

All the CMIP6 models and the observations are re-gridded to a common resolution of 2.5 ◦×2.5 ◦ using a conservative remapping for all physical variables (Jones, 1999). ERA5 and models, including their original grid size, are listed in supplementary table 1.

Jet latitudinal index

To determine the position of the eddy-driven jet, we use an algorithm similar to Blakport and Fyfe (2022). We identify the daily westerly zonal wind speed maxima at 700hPa at each longitude as the "jet-core" speed. The latitude at which the maximum wind speed between 15°N and 75°N is found is considered the latitude of the jet core event. The algorithm is robust to small changes in the latitudinal range. We then calculate the Jet Latitude Index (JLI) as the zonal mean over the NATL area (60 °W to 0 °W) of the latitudinal maxima. To avoid artefacts due to the tilt of the jet stream with latitude, we first identify the speed maxima and its latitude at each longitude before calculating the zonal mean since this method has been shown to remove such artefacts effectively (Blackport and Fyfe, 2022). We also tested additional methods of detecting the jet core, such as prominence detection and using a parabola fit, as in Blackport and Fyfe (2022), which led to similar results.

Persistence calculation

The jet persistence is calculated using the method introduced by Barnes and Hartmann (2010a). In this method, the jet persistence is estimated by calculating the average duration of the jet in a 5° latitude moving window, where the duration is defined by the number of consecutive days the JLI remains within the 5° bounds. Contrary to Barnes and Hartmann (2010a), we only consider events that last at least three consecutive days to calculate the jet average duration. This way, we limit considering false jet core detections associated with strong synoptic systems. However, the results are similar without using a three-day threshold. We analyze the continuous daily timeseries and the seasonal anomalies. For occurrences that overlap different seasons, which roughly happen two times per year in the observational period, the season where the largest number of consecutive days takes place is assigned to the occurrence. Additionally, we also calculate an average persistence value for each model and ERA5 by averaging all the JLI persistent events across their latitudinal distributions. We will refer to this averaged persistence value as "P.AVG".

Transient eddy kinetic energy

We assess the power of synoptic scale transient eddies in the NATL for ERA5 and model data following a methodology similar to Montoya et al., (2021). The method is as follows:

1. The Eddy Kinetic Energy (EKE) from transient eddies is calculated from the 700hPa zonal and meridional wind anomalies:

$$EKE = \frac{1}{2}\left(\overline{u'^2} + \overline{v'^2}\right),$$

where the apostrophe denotes departures from the temporal mean.

2. The EKE is then spatially average over the NATL storm track area, spanning 30°N to 60°N and 60°W to 10°W.

3. The power spectrum of the EKE anomalies is calculated using a multitaper spectrum analysis method (Thomson, 1982; Percival & Walden,1993). The multitaper methodology uses multiple orthogonal tapers (windows) to compute spectral estimates and has been shown to improve the frequency resolution and reduce variance compared to the classical non-parametric Fourier analysis. We chose a tape bandwidth parameter of 2 and 3 tapers since this selection has been shown to be a good compromise between the required frequency resolution and the spectral variance for daily timeseries (e.g., Mann and Park, 1993). The results are not affected by choosing slightly different values for these parameters. .

4. Finally, we extract the power associated with different frequency bands by integrating the power spectrum within these bands.

The results are qualitatively the same, whether using alternative wind levels or slightly adjusting the spatial averaging area.

3. Results

3.1 CMIP6 Persistence Evaluation

In this section, we evaluate the persistence of the jet latitudinal fluctuations in the CMIP6 models and compare it with ERA5.

Fig.1 displays the climatological persistence of the JLI persistent events within 5° latitudinal bins for the HIST period. The results are shown for both the CMIP6 models and ERA5, and the number of persistent events within each bin is also indicated. The P.AVG (an integration of the persistent events across the latitudinal expansion of their distributions across models and observations is shown in the boxplots.

The boxplots in Fig. 1 indicate that most models overestimate the P.AVG throughout all seasons. During winter, models show a mere 5% overestimation compared to observations, but this overestimation increases to about 10% in summer. In spring and autumn, the overestimation reaches approximately 18%. Notably, in the transition seasons, all models consistently overestimate persistence.

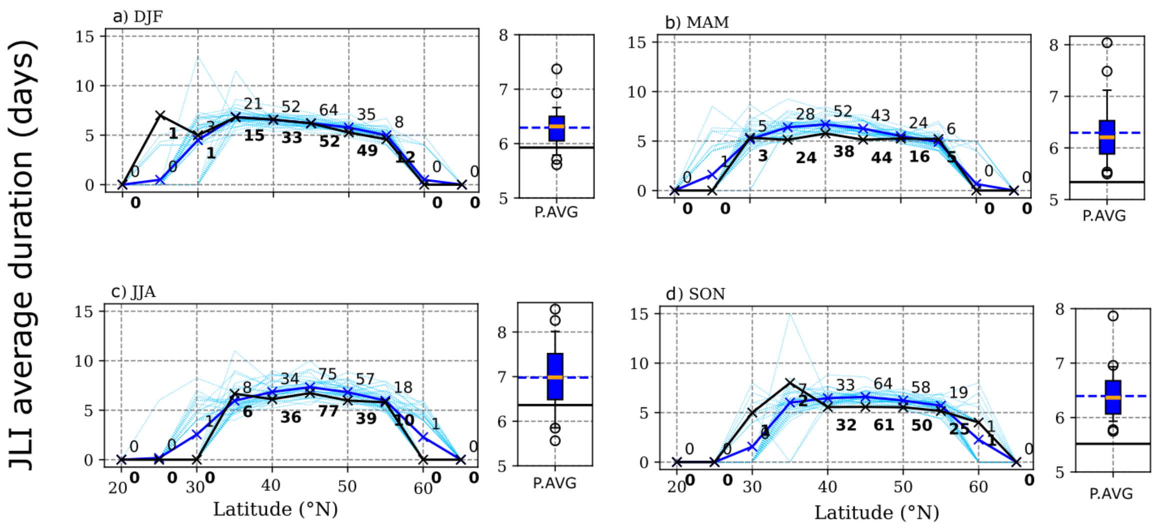

Figure 1: Average duration of the JLI in a moving 5° latitude window for ERA5 (black solid), CMIP6 models (thin dashed blue lines) and the CMIP6 multimodel mean (blue solid line) for the indicated seasons. The number of persistent events is shown above each point. *The b*oxplots illustrat*e* the P.AVG in CMIP6 models. P.AVG is obtained by averaging the durations of all persistent events (lasting >= 3 days) across all latitudinal bins of the left distributions. The blue horizontal dashed line shows the multimodel mean, the orange line within the box shows the median and the solid black line corresponds to ERA5 values.

The persistence distributions suggest that during winter, the model's overestimation of P.AVG is linked to

more persistent events in the central jet locations than observations. However, the average duration of these events across different latitudinal bands within the distribution remains very similar.

During summer, the larger P.AVG can primarily be attributed to more persistent events at the northern parts of the distribution between 50° and 60° (49 events in ERA5 versus 75 events in the multimodel mean). Additionally, the events tend to last slightly longer. In the transition seasons, models exhibit a higher frequency of persistent events and significantly longer durations (approximately 15% longer).

The shape of the persistence distributions does not display the three maxima found in Barnes and Hartmann (2010) for CMIP3 models. We found that this is partially due to the differences in the JLI calculation, which differ from Barnes and Hartmann (2010). We calculate the speed and latitude at each longitude before calculating the zonal mean.

The JLI and, by extension, P.AVG are calculated by zonally averaging the latitudes of the detected jet cores across the NATL. However, the variability of the NATL jet is not limited to latitudinal fluctuations but also includes changes in speed, tilt and meandering (e.g., Eichelberger & Hartmann (2007)). Although the methodology we use to calculate JLI has been shown to reduce the effects of jet tilt variations, we cannot discard that the JLI variability and persistence conflate different phenomena. To assess the impact of these other forms of variability, we recalculated the P.AVG at 2.5 longitude intervals across the NATL and found that the JLI persistence increases slightly towards the center of the NATL (~ 0.5 days) (Fig.S1). This suggests that other types of variability may influence P.AVG, likely changes in the jet tilt. However, the change in persistence across longitudes is small, and the models overestimate persistence across all the longitudinal extent, notably at the eastern side of the NATL, which is the area that is more relevant from an impact point of view. Therefore, we conclude that although other types of variability may affect the persistence calculation, the impact is likely small and does not qualitatively change our conclusions. Additionally, we tested the longitudinal coherence of the jet core latitudinal anomalies by calculating a Hovmöller plot that displays the jet core latitudinal anomalies as a function of time and longitude (Fig.S2) for ERA5. The anomalies show a notable longitudinal coherence, suggesting that longitudinal coherent fluctuations represent an important fraction of the total variability affecting the local latitudinal jet position.

3.2 Persistence relation with the mean state of the jet

Previous studies have shown that the variability and persistence of the jet depend on its latitudinal position during winter (Barnes et al., 2010; Barnes and Hartmann, 2010a; Barnes and Hartmann, 2010b; Kidston & Gerber, 2010). Specifically, these studies show that when the jet is closer to the equator, it tends to have more persistent latitudinal fluctuations than when positioned near the poles. Other research indicates that a strong jet exhibits a more zonal structure and decreased latitudinal fluctuations (Woollings et al., 2018).

Motivated by these findings, we analyze scatterplots between the P.AVG and the mean jet position (Fig. S3a) and velocity and velocity (Fig. S3b) across models and ERA5. A strong relationship between P.AVG and latitude or velocity would imply a potential dependency. However, Fig.S3 reveals no discernible intermodel relationships between latitude or velocity with P.AVG during spring and winter and a statistically significant yet weak positive correlation between summer and autumn. These results apparently differ from Barnes and Hartman (2010) findings. However, it is important to note that this is an intermodel relationship and that for individual model realizations, an equatorward-shifted jet state tends to be more persistent than a poleward-shifted one, as evidenced by the downward slope in Fig. 1a. Additionally, Fig. S3b shows that the models consistently underestimate the jet velocity and models with faster jets tend to be more persistent. However, the correlation coefficients show that this relationship is very weak.

3.3 Synoptic scale waves strength

The results in section 3.1 raise the question of the reasons behind the CMIP6 model JLI overestimation. The EDJ is driven by the convergence of eddy momentum fluxes and the poleward transport of eddy heat, and the largest contribution to this transport comes from the transient eddies associated with baroclinic waves (e.g., Blackmon et al., 1977). Moreover, the latitudinal shifts of the jet are closely linked to Rossby wave breaking on both sides of the jet. Locally, wave breaking induces a deceleration of the eastward flow, thereby shifting the jet poleward when wave breaking occurs on the equatorward side and shifting the jet equatorward when wave breaking occurs on the poleward side (e.g., Barnes and Hartmann, 2012; Kunz et al., 2009; Woollings et al., 2018).

Since synoptic-scale eddies are crucial for the formation and variability of the EDJ (e.g., Barnes and Hartmann, 2011), accurately representing their strength and variability in models is crucial for simulating the EDJ variability. We hypothesize that the overestimation of persistence in models could be associated with too weak synoptic-scale eddies over the NATL.

To investigate this hypothesis, we compare the transient EKE across the NATL in both the models and ERA5. For this analysis, we use the continuous daily time series of HIST. Figure 2a illustrates the transient EKE bias between ERA5 and the CMIP6 multimodel mean, while Figure 2b depicts the EKE bias derived from a 2-6 day bandpass filtered velocity field, representing the contribution of synoptic-scale eddies to EKE. Notably, the CMIP6 ensemble mean exhibits EKE levels between 5% and 15% lower than those in ERA5 (Fig. 2a), while the bandpass filtered EKE is 10% to 20% weaker compared to ERA5 (Fig. 2b). A detailed breakdown of individual model EKE bias is shown in Fig.S4 and 2-6 band pass filtered EKE biases in Fig.S5. Seventeen out of thirty-five models underestimate EKE across the Atlantic, and the rest exhibit an EKE bias pattern, indicating an equatorward mean jet bias. However, the 2-6 day band pass filtered EKE underestimation occurs in all but 4 CMIP6 models, and the bias spatial pattern is spatially homogenous over the NATL. This suggests that the synoptic EKE underestimation is a fundamental model issue and not a product, for example, of mean biases in the jet stream.

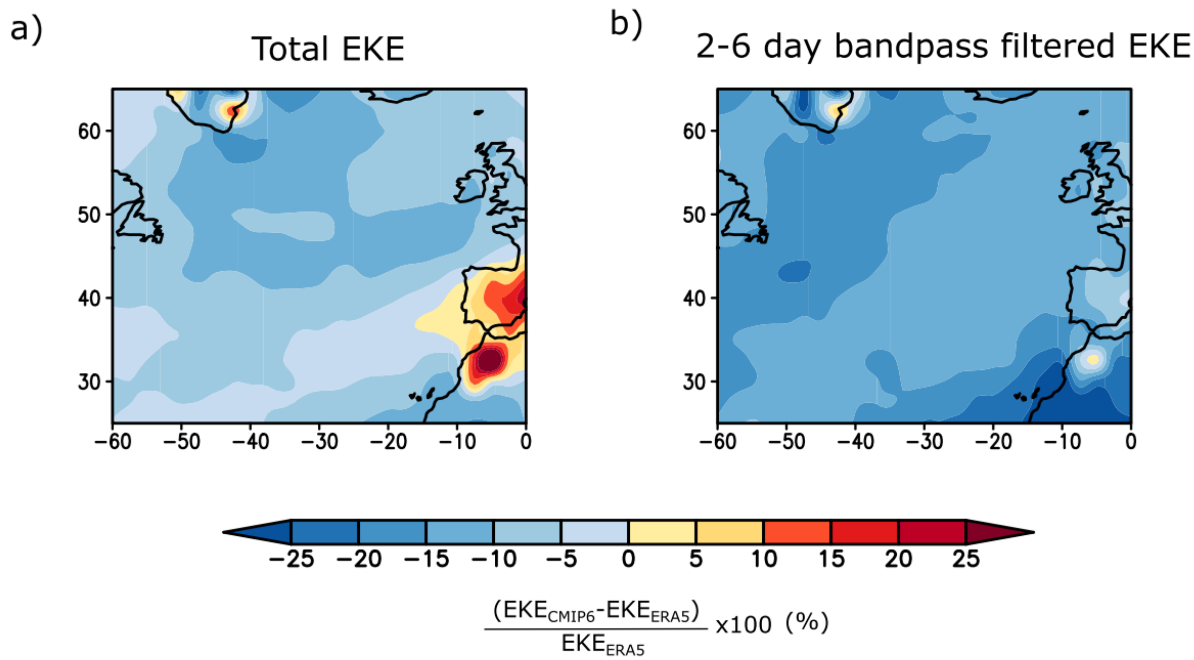

Figure 2: Total EKE bias (a) and synoptic (2-6 day bandpass filtered) EKE bias (b) for the CMIP6 ensemble mean expressed as a percentage.

To better understand the model's EKE representation, we calculate the distribution of EKE power across different frequency ranges (see section 2 for details). Figure 3 shows a box plot illustrating the EKE power for CMIP6 models within “high” frequency bands, with ERA5 power denoted by a red solid dot. The boxplots indicate that most models exhibit inadequate power at high frequencies, including those corresponding to synoptic timescales. Conversely, at "lower" frequencies (>90 days), the models align closely with observations (Fig. S6). These findings suggest that the deficiency in power at high frequencies, particularly at the synoptic scale, within CMIP6 could contribute to the over-persistence of the EDJ over the NATL. A similar underestimation of cyclone intensity has been noted in CMIP5 models (Zappa et al., 2013).

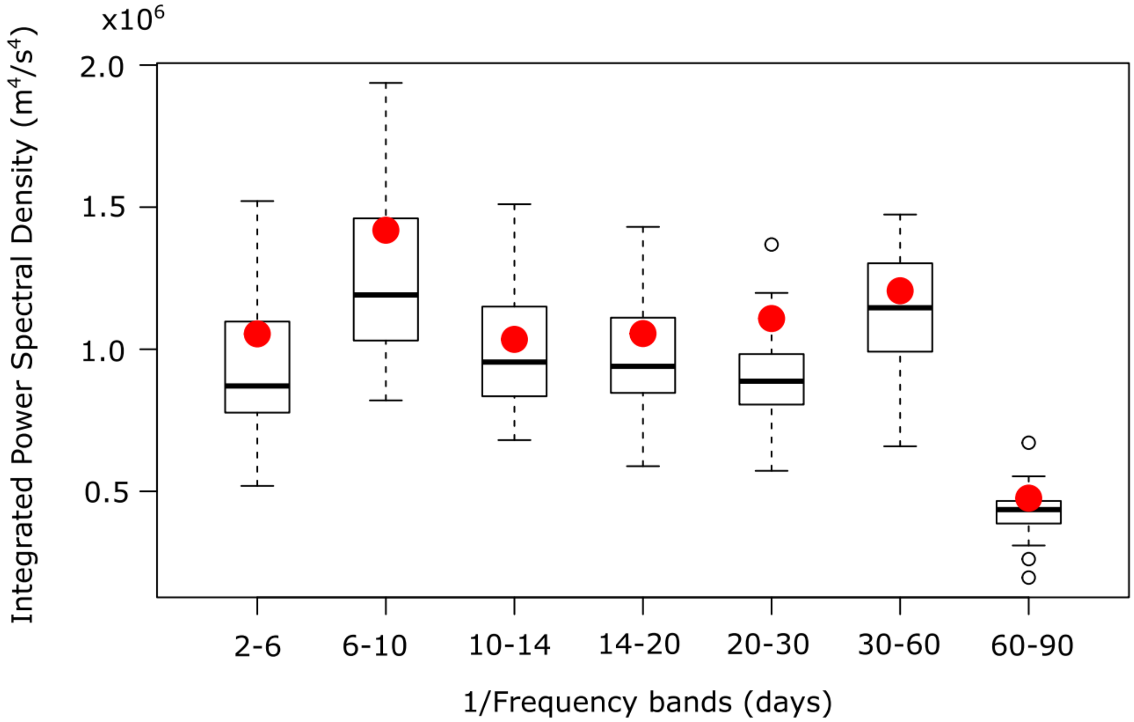

Figure 3: Power spectral density of the EKE spatially average over the NATL (60°W – 10°W, 30°N-60°N) and integrated over the indicated frequency bands for CMIP6 and ERA5 (red solid dot).

3.4 Projected persistence changes

CMIP models project a shift in the zonal mean westerlies towards the poles in response to increasing GHG. However, this shift varies significantly by region and season (e.g., Grise & Polvani, 2014; Simpson et al., 2014; Vallis et al.,2015 for CMIP5 and Harvey et al.,2020 and Oudar et al., 2020 for CMIP6). In the NATL, the jet shifts poleward during summer and autumn but narrows, intensifies, and extends eastward towards Europe in winter (Harvey et al., 2020; Oudar et al., 2020). Jet variability changes are also expected (e.g., Peings et al., 2018), yet projections lack robustness, and the underlying mechanisms driving these alterations remain uncertain (e.g., Hoskins and Woollings, 2015).

Here, we investigate potential changes in persistence using a subset of CMIP6 models under the SSP585 scenario (see methodology). Fig.4 displays the FUT period persistence of JLI persistent events within 5° latitudinal bins. The numbers within each bin represent the count of persistent events in the HIST and FUT periods and their difference. The P.AVG across models for the FUT period is depicted using boxplots, where the red dashed line signifies the FUT multimodel mean, and the blue dashed line represents the HIST multimodel mean.

The box plots highlight significant changes in JJA, indicating an approximate 8% reduction in P.AVG in the future. An individual examination of the models shows that all models, except one, concur on the direction of this change.

The JJA distribution shows a notable decrease in the number of persistent events in the central sections of the distribution, where occurrences are more frequent. Additionally, there is a roughly 10% reduction in the average duration of these events (Fig. S7). This reduction coincides with increased persistent events towards the poleward end of the distribution. However, this increase is insufficient to compensate for the decreased persistence in the central locations.

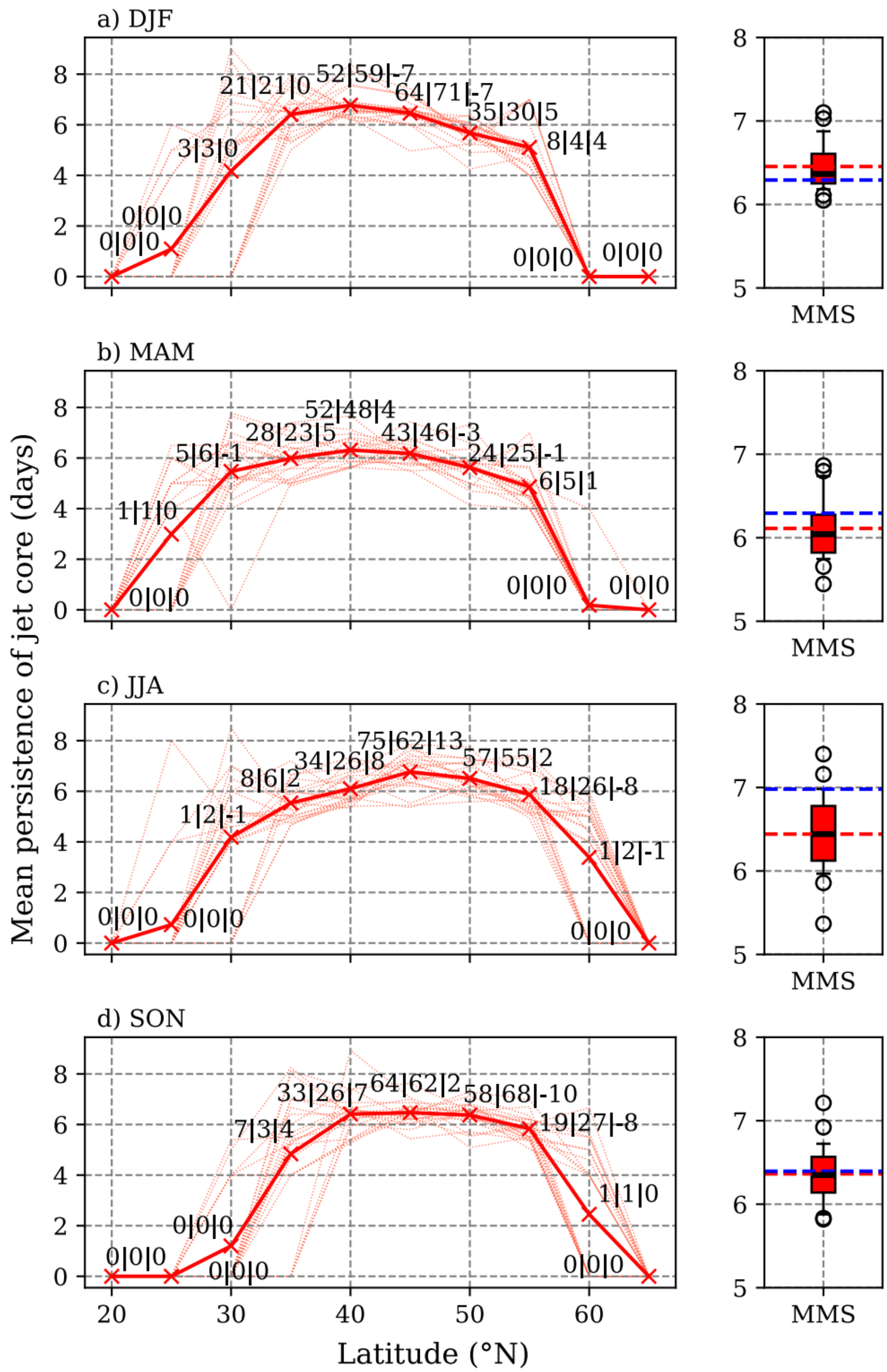

Figure 4: Left column: Average duration of the JLI in a moving 5° latitude window for CMIP6 models forced with the SSP585 scenario (thin dashed red lines) for the indicated seasons. A solid red line shows the multimodel mean. Above each point, the first, second and third numbers indicate the number of persistent events in the HIST and FUT periods and their differences, respectively. Right column: Boxplots illustrating the P.AVG in CMIP6 models. The multimodel mean is shown by a horizontal dashed line for the FUT period (red) and HIST period (blue).

One possible hypothesis accounting for the reduction in persistence at central locations relates to alterations in jet velocity. Previous studies (e.g., Woollings et al., 2018) have linked decreased velocity with heightened jet variability. To scrutinize this hypothesis, we investigated the correlation between model velocity and persistent changes (Fig.S8). Our analysis reveals that 16 out of 20 models project a deceleration of the jet during summer. Furthermore, a robust relationship emerges between velocity and persistence alterations: models predicting larger speed reductions also indicate more substantial decreases in persistence.

The observed increase in persistence towards the poleward side of the distributions could be attributed to the poleward shift of the jet during summer. Various studies have shown evidence that as the jet migrates poleward, its variability transitions from shifting to a more pulsing mode, consequently leading to a decrease in the persistence of anomalous meridional shifts (Kidston & Gerber, 2010; Barnes et al., 2010; Barnes and Hartmann, 2010; Barnes and Hartmann, 2011).

4. Conclusions and discussion

This study focused on analyzing the persistence of North Atlantic jet latitudinal fluctuations across a set of CMIP6 models and ERA5 data. The key findings are summarized below:

- CMIP6 models consistently overestimate the persistence of the jet latitudinal fluctuations during the historical period.
- The evidence suggests that scale model over-persistence is associated with too weak EKE power at high frequencies, particularly at the synoptic scales.
- By the end of the XXI century, CMIP6 models project a decrease in jet persistence of about 10% during summer and no significant change in the other seasons.
- The projected decrease in summer persistence is correlated with a decrease in jet velocity.

Finally, the representation of jet persistence in models strongly correlates with their depiction of the persistence of impact-related variables like precipitation (see Fig.S9). Understanding how the biases reported in this study impact the projections of persistent events, especially extreme events, is crucial to improving and constraining the uncertainty in regional climate change projections. Additionally, understanding the reasons behind these model biases and exploring avenues to reduce them should be considered by model developers. Furthermore, future research should investigate the relationship between these findings and the so-called “signal-to-noise paradox” (e.g., Scaife and Smith, 2018).

Acknowledgements

We would like to thank Tim Woollings from the University of Oxford for the valuable discussions and suggestions. Funding for Open access is provided by the University of Graz.

Conflict of Interest

The authors declare no conflicts of interest relevant to this study.

Open Research

ERA5 data description can be found in Hersbach et al., (2020) and was downloaded from the Copernicus Climate Change Service (C3S) at Hersbach et al., (2023). CMIP6 data is described in Eyring et al., (2016) and was downloaded from Copernicus Climate Change Service, Climate Data Store, (2021). The models used in this study are listed in Table S1. The code used in this study is available via personal request to the corresponding author.

References

Barnes, E. A., D. L. Hartmann, D. M. W. Frierson, and J. Kidston, (2010). Effect of latitude on the persistence of eddy-driven jets. *Geophys. Res. Lett.*, 37, L11804, doi:10.1029/2010GL043199.

Barnes, E. A., and Hartmann, D. L. (2010a). Testing a theory for the effect of latitude on the persistence of eddy-driven jets using CMIP3 simulations. *Geophys. Res. Lett*., 37, L15801, doi:10.1029/2010GL044144.

Barnes, E. A., and Hartmann, D. L. (2010b). Influence of eddy-driven jet latitude on North Atlantic jet persistence and blocking frequency in CMIP3 integrations. *Geophys. Res. Lett.*, 37, L23802, doi:10.1029/2010GL045700.

Barnes, E. A., and D. L. Hartmann (2011). Rossby Wave Scales, Propagation, and the Variability of Eddy-Driven Jets. *J. Atmos. Sci*., 68, 2893–2908, https://doi.org/10.1175/JAS-D-11-039.1.

Barnes, E. A., and D. L. Hartmann (2012). Detection of Rossby wave breaking and its response to shifts of the midlatitude jet with climate change. *J. Geophys. Res*., 117, D09117, doi:10.1029/2012JD017469.

Blackburn, M., Methven, J. and Roberts, N. (2008). Large-scale context for the UK floods in summer 2007. *Weather*, 63: 280-288. https://doi.org/10.1002/wea.322.

Blackmon, M. L., J. M. Wallace, N. Lau, and S. L. Mullen (1977). An Observational Study of the Northern Hemisphere Wintertime Circulation. *J. Atmos. Sci.*, 34, 1040–1053, https://doi.org/10.1175/1520-0469(1977)034<1040:AOSOTN>2.0.CO;2.

Blackport, R., Screen, JA (2020). Weakened evidence for mid-latitude impacts of Arctic warming. *Nat. Clim. Chang.* 10, 1065–1066. https://doi.org/10.1038/s41558-020-00954-y.

Blackport R. and J. Fyfe (2022). Climate models fail to capture strengthening wintertime North Atlantic jet and impacts on Europe. *Sci. Adv.*8,eabn3112.DOI:10.1126/sciadv.abn3112.

Cattiaux, J., R. Vautard, C. Cassou, P. Yiou, V. Masson-Delmotte, and F. Codron (2010). Winter 2010 in Europe: A cold extreme in a warming climate. *Geophys. Res. Lett.*, 37, L20704, doi:10.1029/2010GL044613.

Cattiaux, J., Peings, Y., Saint-Martin, D., Trou-Kechout, N., and Vavrus, S. J. (2016). Sinuosity of midlatitude atmospheric flow in a warming world. *Geophys. Res. Lett*., 43, 8259–8268, doi:10.1002/2016GL070309.

Copernicus Climate Change Service, Climate Data Store, (2021): CMIP6 climate projections. Copernicus Climate Change Service (C3S) Climate Data Store (CDS). DOI: 10.24381/cds.c866074c.

Coumou, D., Rahmstorf. S. (2012). A decade of weather extremes. *Nature Clim Change* 2, 491–496. https://doi.org/10.1038/nclimate1452.

Dim Coumou et al., (2015). The weakening summer circulation in the Northern Hemisphere mid-latitudes. *Science* 348,324-327.DOI:10.1126/science.1261768.

Dunn-Sigouin, E., and S.-W. Son (2013). Northern Hemisphere blocking frequency and duration in the CMIP5 models. *J. Geophys. Res. Atmos*., 118, 1179–1188, doi:10.1002/jgrd.50143.

Eichelberger, S. J., & Hartmann, D. L. (2007). Zonal Jet Structure and the Leading Mode of Variability. Journal of Climate, 20(20), 5149-5163. https://doi.org/10.1175/JCLI4279.1.

Eyring, V., Bony, S., Meehl, G. A., Senior, C. A., Stevens, B., Stouffer, R. J., and Taylor, K. E.: Overview of the Coupled Model Intercomparison Project Phase 6 (CMIP6) experimental design and organization, Geosci. Model Dev., 9, 1937–1958. [https://cds.climate.copernicus.eu/cdsapp#!/dataset/projections-cmip6?tab=overview]. https://doi.org/10.5194/gmd-9-1937-2016, 2016.

Fischer, E., Knutti, R. (2015). Anthropogenic contribution to global occurrence of heavy-precipitation and high-temperature extremes. *Nature Clim Change* 5, 560–564. https://doi.org/10.1038/nclimate2617.

Francis, J.A., Vavrus, S.J. and Cohen, J. (2017). Amplified Arctic warming and mid-latitude weather: new perspectives on emerging connections. *WIREs Clim Change*, 8: e474. https://doi.org/10.1002/wcc.474.

Francis, J. A., Skific, N., & Vavrus, S. J. (2018). North American weather regimes are becoming more persistent: Is Arctic amplification a factor? *Geophysical Research Letters*, 45, 11,414–11,422. https://doi.org/10.1029/2018GL080252.

Francis, J.A., Skific, N. & Vavrus, S.J. (2020). Increased persistence of large-scale circulation regimes over Asia in the era of amplified Arctic warming, past and future. *Sci Rep* 10, 14953. https://doi.org/10.1038/s41598-020-71945-4.

Galfi, V. M., & Messori, G. (2023). Persistent anomalies of the North Atlantic jet stream and associated surface extremes over Europe. Environmental Research Letters, 18(2), 024017. 024017DOI 10.1088/1748-9326/acaedf.

Di Capua, G., & Coumou, D. (2016). Changes in meandering of the Northern Hemisphere circulation. Environmental Research Letters, 11(9), 094028. DOI 10.1088/1748-9326/11/9/094028.

Grise, K. M., and Polvani, L. M. (2014). The response of midlatitude jets to increased CO2: Distinguishing the roles of sea surface temperature and direct radiative forcing. *Geophys. Res. Lett*., 41, 6863– 6871, doi:10.1002/2014GL061638.

Harvey, B. J., Cook, P., Shaffrey, L. C., & Schiemann, R. (2020). The response of the northern hemisphere storm tracks and jet streams to climate change in the CMIP3, CMIP5, and CMIP6 climate models. *Journal of Geophysical Research: Atmospheres*, 125, e2020JD032701. https://doi.org/10.1029/2020JD032701.

Hassanzadeh, P., Z. Kuang, and B. F. Farrell (2014). Responses of midlatitude blocks and wave amplitude to changes in the meridional temperature gradient in an idealized dry GCM. *Geophys. Res. Lett*., 41, 5223–5232, doi:10.1002/2014GL060764.

Hersbach, H., Bell, B., Berrisford, P., Biavati, G., Horányi, A., Muñoz Sabater, J., Nicolas, J., Peubey, C., Radu, R., Rozum, I., Schepers, D., Simmons, A., Soci, C., Dee, D., Thépaut, J-N. (2023): ERA5 monthly averaged data on single levels from 1940 to present. Copernicus Climate Change Service (C3S) Climate Data Store (CDS), DOI: 10.24381/cds.f17050d7.

Hersbach H, Bell B, Berrisford P, et al. (2020). The ERA5 global reanalysis. *Q J R Meteorol Soc.*146: 1999–2049, https://doi.org/10.1002/qj.3803.

Hoskins, B., Woollings, T. (2015). Persistent Extratropical Regimes and Climate Extremes. *Curr Clim Change Rep* 1, 115–124. https://doi.org/10.1007/s40641-015-0020-8.

Jones, P. W., (1999). First- and Second-Order Conservative Remapping Schemes for Grids in Spherical Coordinates. *Mon. Wea. Rev.*, 127, 2204–2210, https://doi.org/10.1175/1520-0493(1999)127<2204:FASOCR>2.0.CO;2.

Kidston, J., and Gerber, E. P. (2010). Intermodel variability of the poleward shift of the austral jet stream in the CMIP3 integrations linked to biases in 20th century climatology. *Geophys. Res. Lett*., 37, L09708, doi:10.1029/2010GL042873.

Kornhuber, K., V. Petoukhov, D. Karoly, S. Petri, S. Rahmstorf, and D. Coumou, (2017). Summertime Planetary Wave Resonance in the Northern and Southern Hemispheres. *J. Climate*, 30, 6133–6150, https://doi.org/10.1175/JCLI-D-16-0703.1.

Kunz, T., Fraedrich, K. and Lunkeit, F. (2009). Synoptic scale wave breaking and its potential to drive NAO-like circulation dipoles: A simplified GCM approach. *Q.J.R. Meteorol. Soc*., 135: 1-19. https://doi.org/10.1002/qj.351.

Li, J., Thompson, D.W.J. (2021). Widespread changes in surface temperature persistence under climate change. *Nature* 599, 425–430. https://doi.org/10.1038/s41586-021-03943-z.

Mahlstein, I., O. Martius, C. Chevalier, and D. Ginsbourger (2012). Changes in the odds of extreme events in the Atlantic basin depending on the position of the extratropical jet. *Geophys. Res. Lett*., 39, L22805,
doi:10.1029/2012GL053993.

Mann, M. E., & Park, J. (1993). Spatial correlations of interdecadal variation in global surface temperatures. *Geophysical Research Letters, 20*(11), 1055-1058, https://doi.org/10.1029/93GL00752.

Masato, G., B. J. Hoskins, and T. Woollings, (2013). Winter and Summer Northern Hemisphere Blocking in CMIP5 Models. *J. Climate*, 26, 7044–7059, https://doi.org/10.1175/JCLI-D-12-00466.1.

Matsueda, M., R. Mizuta, and S. Kusunoki, (2009). Future change in wintertime atmospheric blocking simulated using a 20-km-mesh atmospheric global circulation model. *J. Geophys. Res*., 114, D12114, doi:10.1029/2009JD011919.

Montoya Duque, E., Lunkeit, F. & Blender, R., (2021). North Atlantic midwinter storm track suppression and the European weather response in ERA5 reanalysis. *Theor Appl Climatol* 144, 839–845. https://doi.org/10.1007/s00704-021-03517-z.

O'Neill, B.C., Kriegler, E., Riahi, K. et al.,(2014). A new scenario framework for climate change research: the concept of shared socioeconomic pathways. *Climatic Change* 122, 387–400. https://doi.org/10.1007/s10584-013-0905-2.

Oudar, T., Cattiaux, J., & Douville, H. (2020). Drivers of the northern extratropical eddy-driven jet change in CMIP5 and CMIP6 models. *Geophysical Research Letters*, 47, e2019GL086695. https://doi.org/10.1029/2019GL086695.

Peings, Y., Cattiaux, J., Vavrus, S. J. & Magnusdottir, G. (2018) Projected squeezing of the wintertime North-Atlantic jet. Environ. Res. Lett. 13, 074016.

Percival DB, Walden AT. *Spectral Analysis for Physical Applications*. Cambridge University Press; 1993.

Pfleiderer, P., Coumou, D., (2018). Quantification of temperature persistence over the Northern Hemisphere land-area. *Clim Dyn* 51, 627–637. https://doi.org/10.1007/s00382-017-3945-x.

Scaife, A.A., Smith, D (2018). A signal-to-noise paradox in climate science. *npj Clim Atmos Sci* 1, 28. https://doi.org/10.1038/s41612-018-0038-4.

Simpson, I. R., T. A. Shaw, and R. Seager, (2014). A Diagnosis of the Seasonally and Longitudinally Varying Midlatitude Circulation Response to Global Warming. *J. Atmos. Sci*., 71, 2489–2515, https://doi.org/10.1175/JAS-D-13-0325.1.

Thomson, D.J. (1982) Spectrum Estimation and Harmonic Analysis. Proceedings of the IEEE, 70, 1055-1096. https://doi.org/10.1109/PROC.1982.12433

Smith, D.M., Eade, R., Andrews, M.B. et al. Robust but weak winter atmospheric circulation response to future Arctic sea ice loss. Nat Commun 13, 727 (2022). https://doi.org/10.1038/s41467-022-28283-y

Trigo, Ricardo & Añel, J.A. & Barriopedro, David & García-Herrera, Ricardo & Gimeno, Luis & Nieto, Raquel & Castillo, Rodrigo & Allen, M.R. & Massey, N.. (2013). The record winter drought of 2011–2012 in the Iberian Peninsula. *Bull. Am. Meteorol. Soc*.. 94. S41-S45.

Tuel, A. and Martius, O.,(2023). Weather persistence on sub-seasonal to seasonal timescales: a methodological review. *Earth Syst. Dynam*., 14, 955–987, https://doi.org/10.5194/esd-14-955-2023.

Vallis, G.K., Zurita-Gotor, P., Cairns, C. and Kidston, J. (2015). Response of the large-scale structure of the atmosphere to global warming. *Q.J.R. Meteorol. Soc*., 141: 1479-1501. https://doi.org/10.1002/qj.2456.

Woollings, T., Barnes, E., Hoskins, B., Kwon, Y., Lee, R. W., Li, C., Madonna, E., McGraw, M., Parker, T., Rodrigues, R., Spensberger, C., & Williams, K. (2018). Daily to Decadal Modulation of Jet Variability. *Journal of Climate*, 31(4), 1297-1314. https://doi.org/10.1175/JCLI-D-17-0286.1.

Zappa, G., L. C. Shaffrey, K. I. Hodges, P. G. Sansom, and D. B. Stephenson, (2013). A Multimodel Assessment of Future Projections of North Atlantic and European Extratropical Cyclones in the CMIP5 Climate Models. *J. Climate, 26*, 5846–5862, https://doi.org/10.1175/JCLI-D-12-00573.1.

Figure 1.

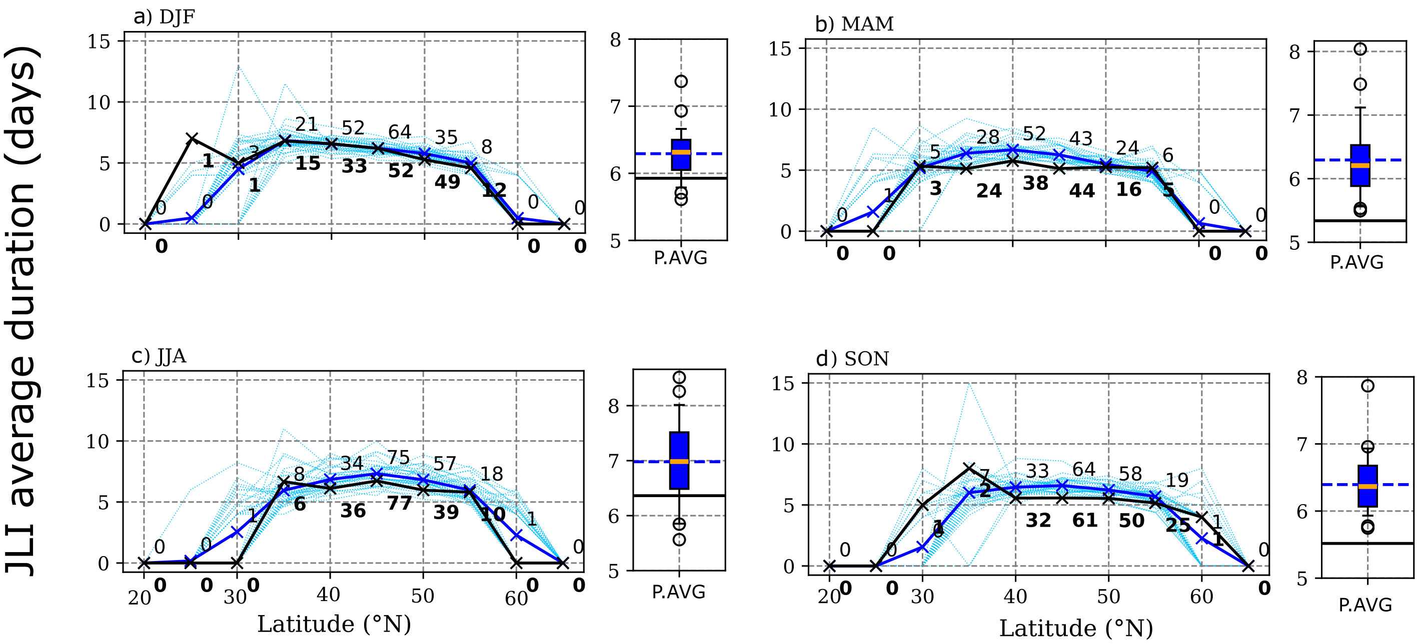

JLI average duration (days)
a) DJF
b) MAM
c) JJA
d) SON
P.AVG
Latitude (°N)

Figure 2.

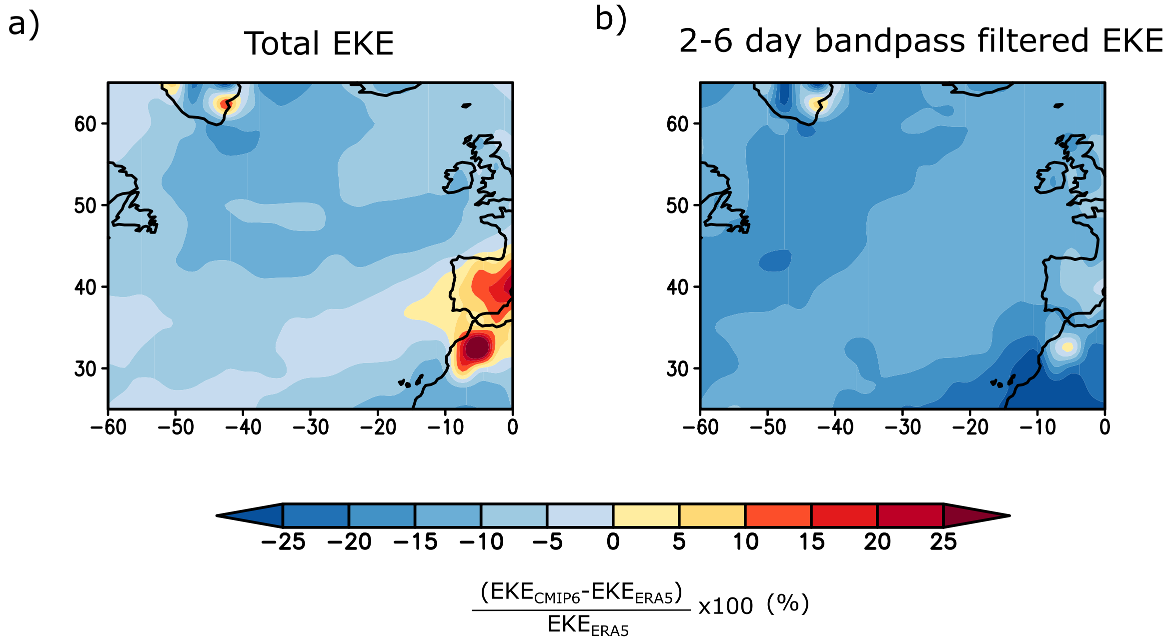

a)
Total EKE
b)
2-6 day bandpass filtered EKE
60
50
40
30
−60 −50 −40 −30 −20 −10 0
−25 −20 −15 −10 −5 0 5 10 15 20 25
$\frac{(EKE_{CMIP6}-EKE_{ERA5})}{EKE_{ERA5}}$ x100 (%)

Figure 3.

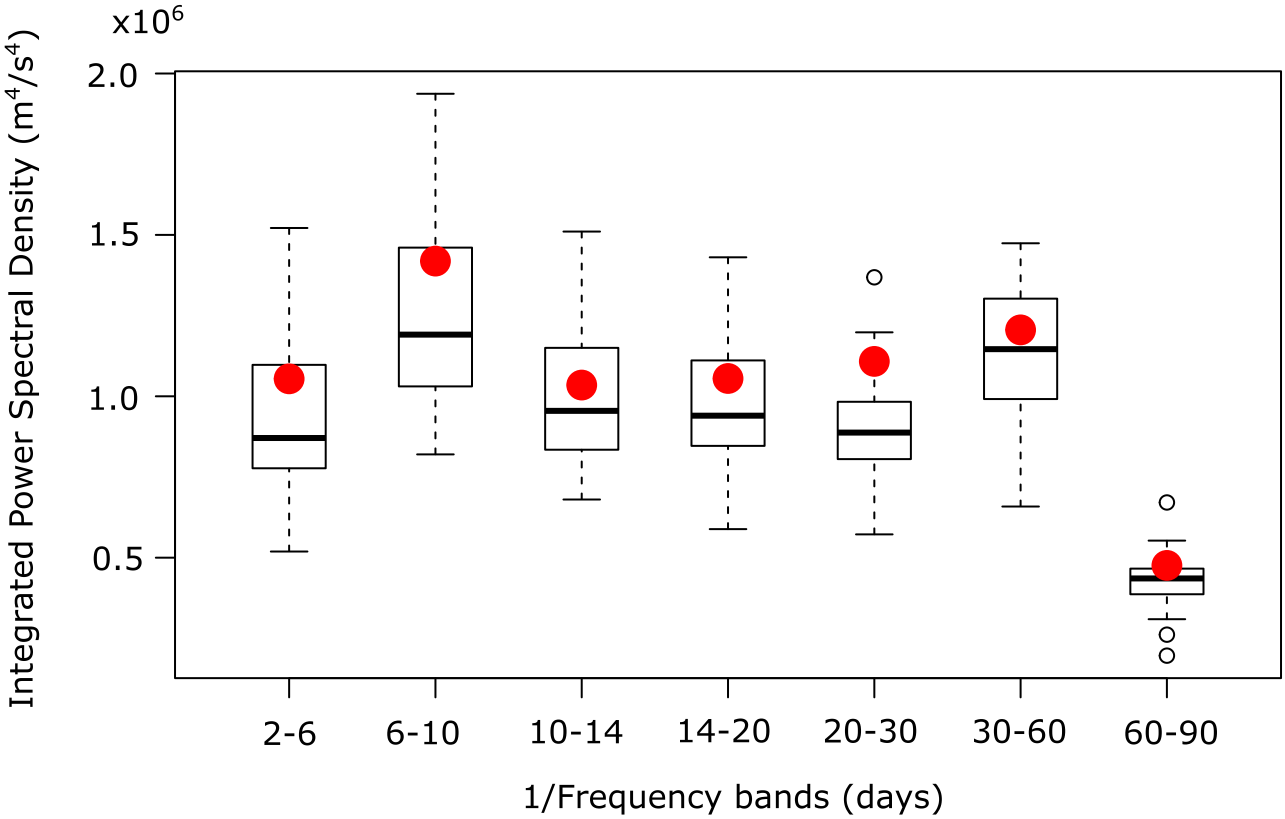

x10^6
Integrated Power Spectral Density (m^4/s^4)
2.0
1.5
1.0
0.5
2-6
6-10
10-14
14-20
20-30
30-60
60-90
1/Frequency bands (days)

Figure 4.

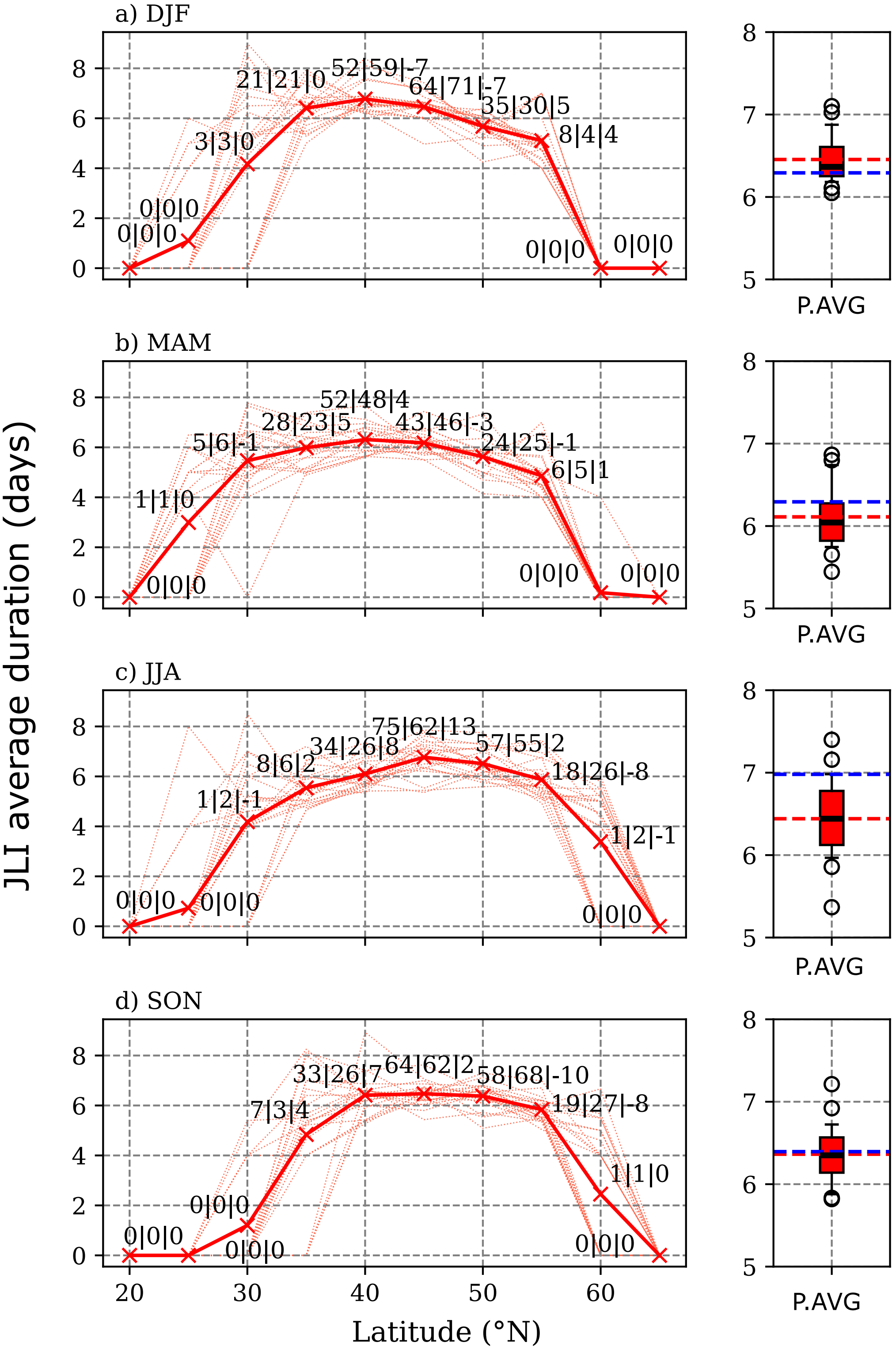
a) DJF
b) MAM
c) JJA
d) SON
JLI average duration (days)
Latitude (°N)
P.AVG
0|0|0
0|0|0
3|3|0
21|21|0
52|59|-7
64|71|-7
35|30|5
8|4|4
0|0|0
0|0|0
1|1|0
0|0|0
5|6|-1
28|23|5
52|48|4
43|46|-3
24|25|-1
6|5|1
0|0|0
0|0|0
0|0|0
0|0|0
1|2|-1
8|6|2
34|26|8
75|62|13
57|55|2
18|26|-8
1|2|-1
0|0|0
0|0|0
0|0|0
0|0|0
7|3|4
33|26|7
64|62|2
58|68|-10
19|27|-8
1|1|0
0|0|0

AGU PUBLICATIONS

[Geophysical Research Letters]

Supporting Information for

CMIP6 Models Overestimate the North Atlantic Eddy-Driven Jet Persistence

Albert Ossó[1] and Florian Ennemoser[1]

[1] Wegener Center for Climate and Global Change, University of Graz, Graz, Austria

Corresponding author: Albert Ossó (albert.osso-castillon@uni-graz.at)

Contents of this file

Figures S1 to S9
Tables S1

Additional Supporting Information (Files uploaded separately)

Captions for Tables S1

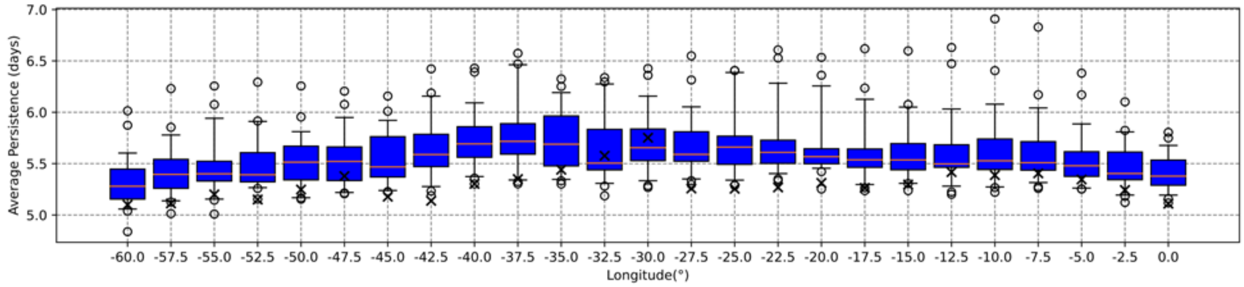

Figure S1: Boxplots illustrating the P.AVG for 2.5 longitudinal intervals across the NATL for CMIP6 models and ERA5. The orange line within the box shows the CMIP6 median and the solid black crosses show ERA5 values.

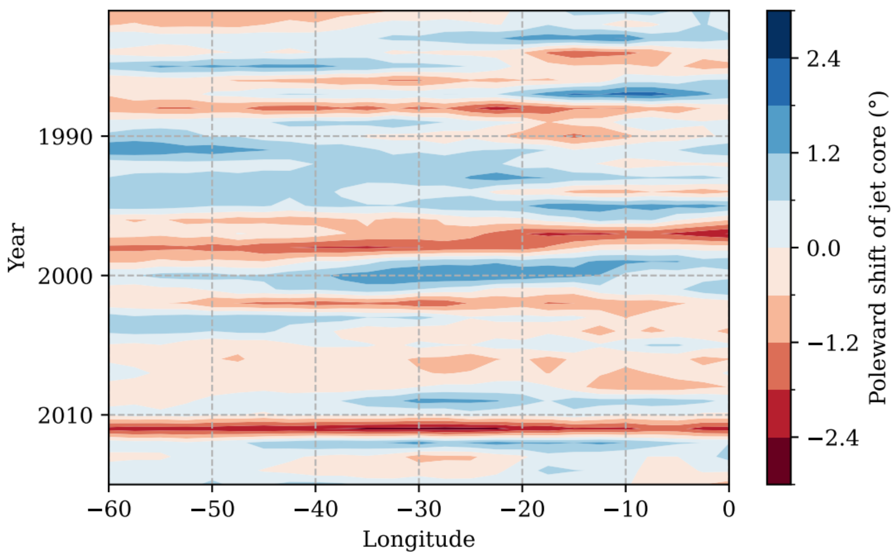

Figure S2: Jet core latitudinal anomalies as a function of time and longitude for ERA5.

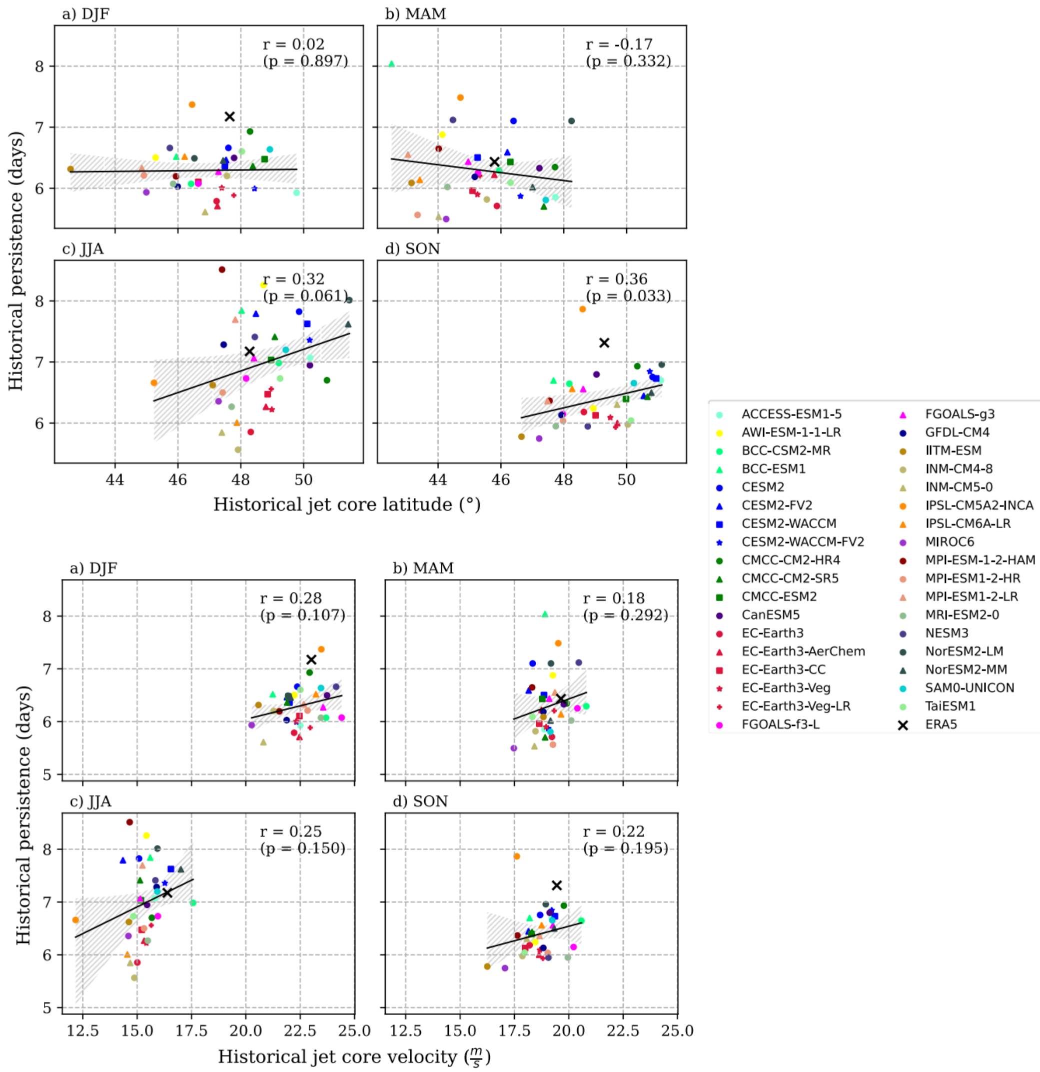

Figure S3: Left column: Scatter plot between P.AVG and the jet mean latitudinal position during the HIST period. CMIP6 models are shown by coloured symbols. Models from the same institution are indicated by the similarity of colours. The black cross shows ERA5. The solid black line is the regressed linear fit, with a hatched 95th percentile confidence interval estimated with a 10000 bootstrap resampling test. Additionally, the correlation value r and the p-value are shown. Right column: As left but for the jet mean velocity.

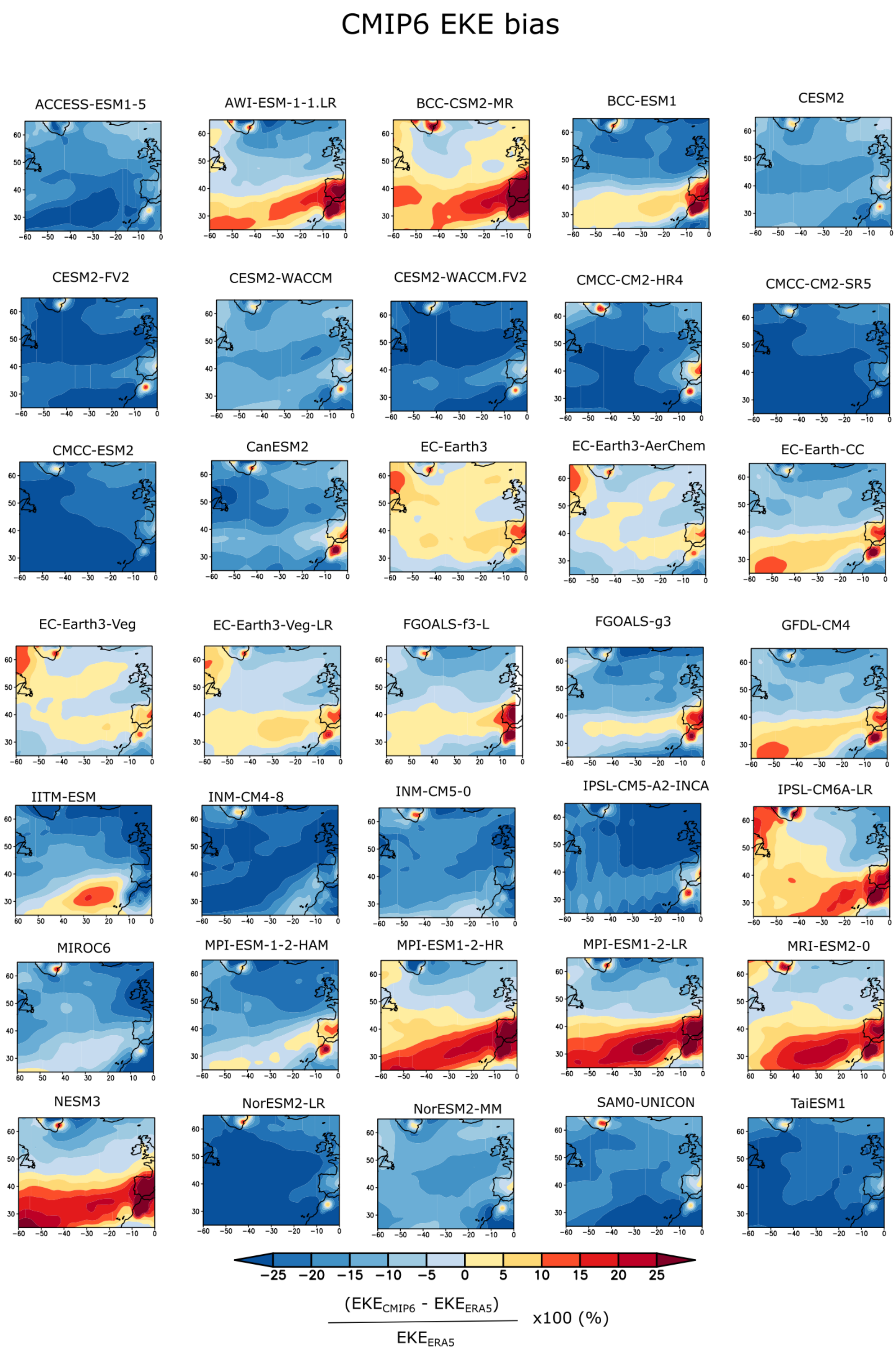

Figure S4: EKE bias for the CMIP6 models expressed as a percentage.

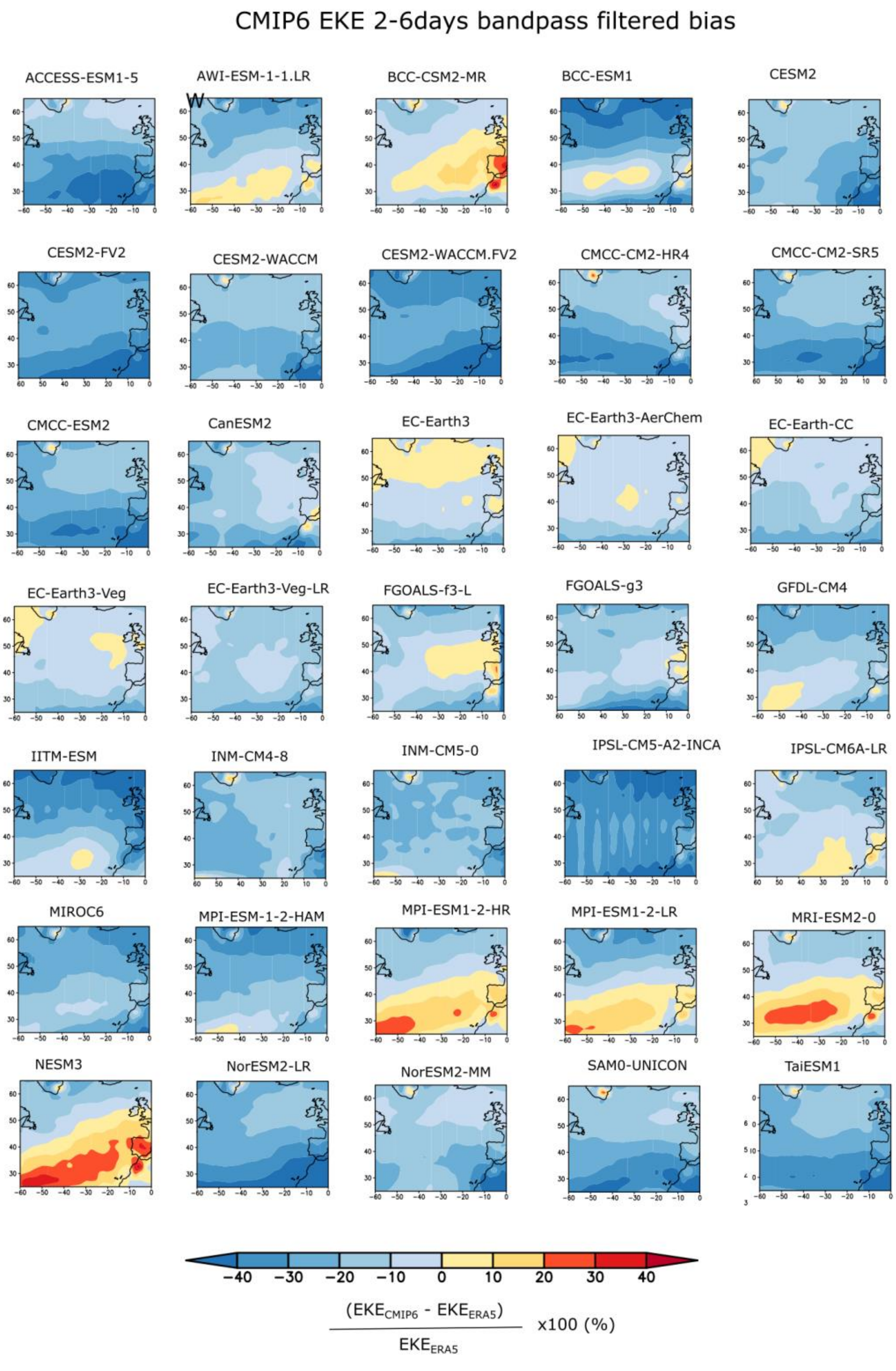

Figure S5: 2-6 day bandpass filtered EKE bias for the CMIP6 models expressed as a percentage.

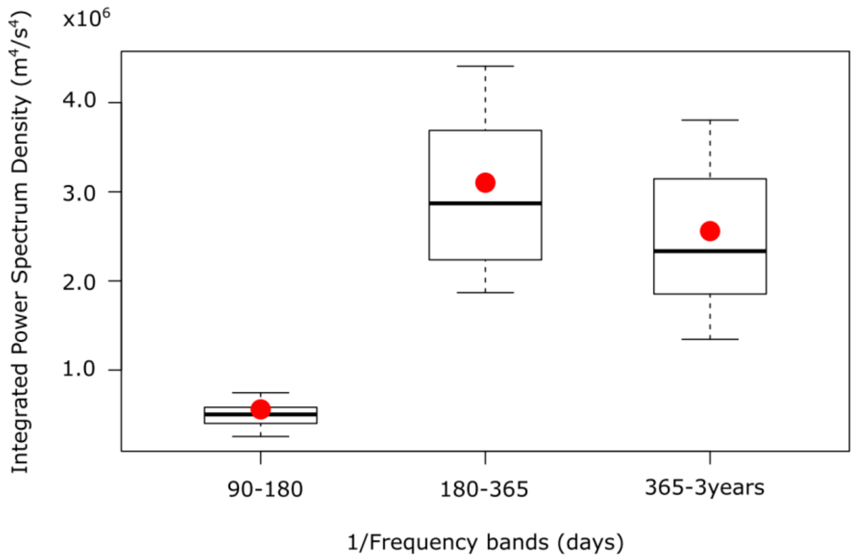

Figure S6: Power spectral density of the EKE spatially average over the NATL (60°W – 10°W, 30°N-60°N) and integrated over the indicated frequency bands for CMIP6 and ERA5 (red solid dot).

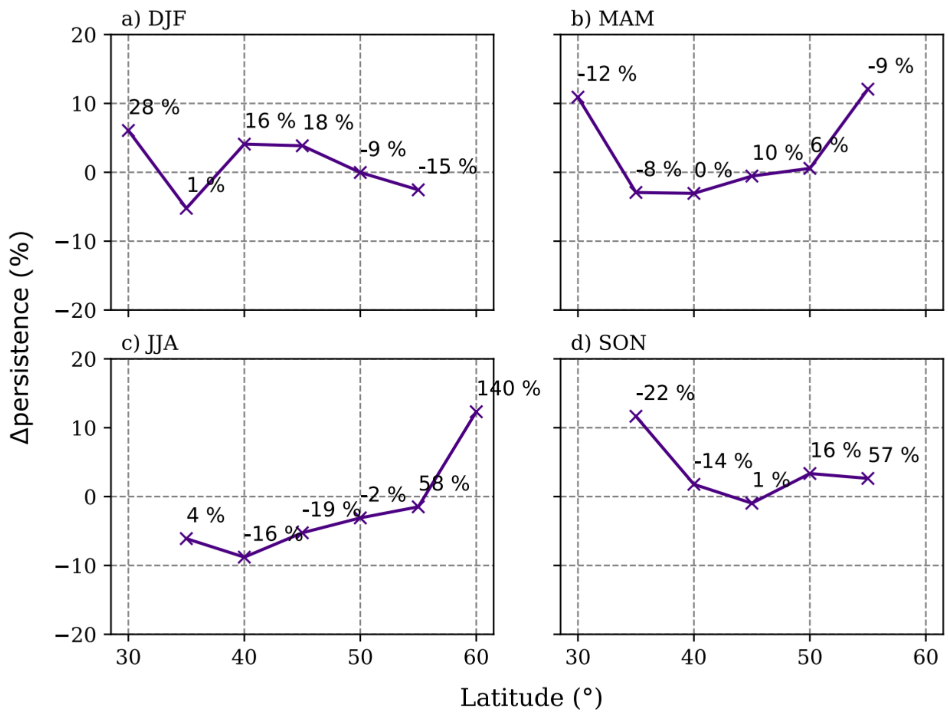

Figure S7. Δpersistence is the CMIP6 multimodel mean difference between the average duration of the JLI for the FUT and HIST periods in a moving 5° latitude window for the indicated seasons. The difference is normalized with the JLI duration in the HIST period and expressed as a percentage. The difference in the number of persistent events between the FUT and HIST periods at each bin is shown above each point and expressed as a percentage. The extremes of the distribution containing less than one event in the HIST or FUT period have been removed.

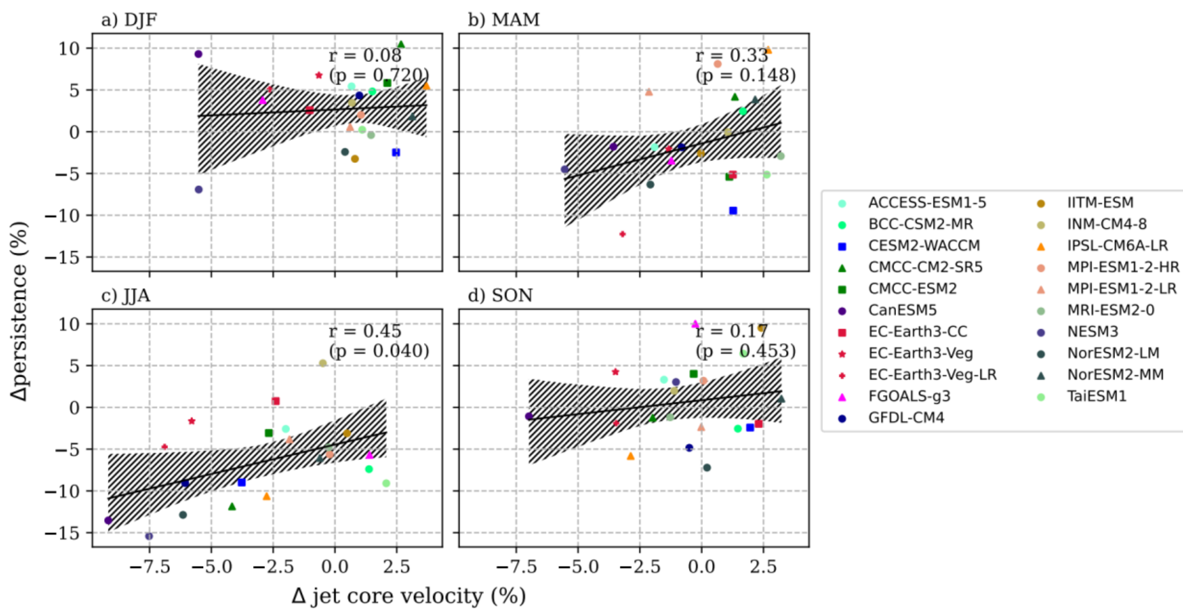

Figure S8: Scatter plots between P.AVG (FUT) - P.AVG(HIST) and Vel(FUT) - Vel(HIST). Colored symbols show CMIP6 models. The similarity of colors indicates models from the same institution. The solid black line is the regressed linear fit, with a hatched 95th percentile confidence interval estimated with a 10000 bootstrap resampling test. Additionally, the correlation value r and the p-value are shown.

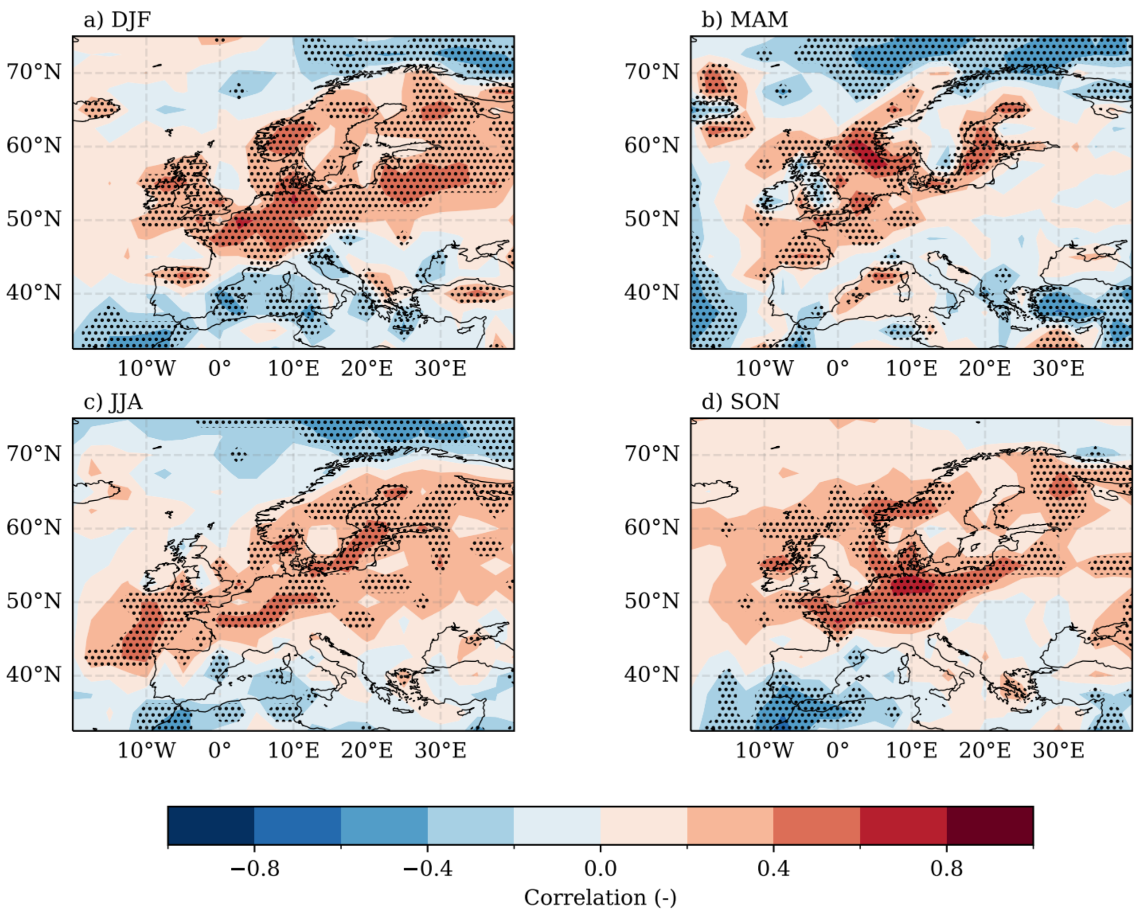

Figure S9. Each grid point displays the correlation (r) between the average precipitation duration CMIP6 intermodel spread and the jet P.AVG intermodel spread during the HIST period. Note that the square of r would indicate the fraction of the intermodel precipitation duration spread explained by the jet P.AVG model spread. The precipitation duration is calculated for each model and grid point as the number of consecutive days with at least 1mm of precipitation. Stippling indicates correlation values statistically significant at the 90% level.

	Model name	Institution	Original atmospheric gridsize (longitude × latitude)
1	***ACCESS-ESM1-5***	Australian Community Climate and Earth System Simulator	1.875 × 1.25
2	AWI-ESM-1-1-LR	Alfred Wegener Institue Helmholtz Centre of Polar and Marine Research	1.875 × 1.25
3	***BCC-CSM2-MR***	Beijing Climate Center	1.125 × 1.125
4	BCC-ESM1	Beijing Climate Center	2.8125 × 2.8125
5	***CanESM5***	Canadian Centre for Climate Modelling and Analysis, Environment and Climate Change	2.8125 × 2.8125
6	CESM2	National Center for Atmospheric Research Climate and Global Dynamics Laboratory	1.0 × 1.0
7	CESM2-FV2	National Center for Atmospheric Research Climate and Global Dynamics Laboratory	2.5 × 1.8
8	***CESM2-WACCM***	National Center for Atmospheric Research Climate and Global Dynamics Laboratory	1.25 × 0.9375
9	CESM2-WACCM-FV2	National Center for Atmospheric Research Climate and Global Dynamics Laboratory	2.5 × 1.875
10	CMCC-CM2-HR4	Fondazione Centro Euro-Mediterraneo sui Cambiamenti Climatici	1.25 × 0.9375
11	***CMCC-CM2-SR5***	Fondazione Centro Euro-Mediterraneo sui Cambiamenti Climatici	1.25 × 0.9375
12	***CMCC-ESM2***	Fondazione Centro Euro-Mediterraneo sui Cambiamenti Climatici	1.25 × 0.9375
13	EC-Earth3	EC-Earth consortium, Rossby Center, Swedish Meteorological and Hydrological Institute	0.703125 × 0.703125
14	EC-Earth3-AerChem	EC-Earth consortium, Rossby Center, Swedish Meteorological and Hydrological Institute	0.703125 × 0.703125
15	***EC-Earth3-CC***	EC-Earth consortium, Rossby Center, Swedish Meteorological and Hydrological Institute	0.703125 × 0.703125
16	***EC-Earth3-Veg***	EC-Earth consortium, Rossby Center, Swedish Meteorological and Hydrological Institute	0.703125 × 0.703125
17	***EC-Earth3-Veg-LR***	EC-Earth consortium, Rossby Center, Swedish Meteorological and Hydrological Institute	0.703125 × 0.703125
18	FGOALS-f3-L	Chinese Academy of Sciences	1.0 × 1.0
19	***FGOALS-g3***	Chinese Academy of Sciences	2.0 × 2.25
20	***GFDL-CM4***	National Oceanic and Atmospheric Administration Geophysical Fluid Dynamics Laboratory	1.0 × 1.0
21	***IITM-ESM***	Indian Institute for Tropical Meteorology	1.875 × 1.915
22	***INM-CM4-8***	Institute for Numerical Mathematics Russian Academy of Science	2.0 × 1.5
23	INM-CM5-0	Institute for Numerical Mathematics Russian Academy of Science	2.0 × 1.5
24	***IPSL-CM6A-LR***	Institute Pierre Simon Laplace	2.5 × 1.267606
25	IPSL-CM6A-LR-INCA	Institute Pierre Simon Laplace	2.5 × 1.267606
26	MIROC6	Japan Agency for Marine-Earth Science and Technology	1.40625 × 1.40625
27	MPI-ESM-1-2-HAM	Max Planck Institute for Meteorology	1.875 × 1.875
28	***MPI-ESM1-2-HR***	Max Planck Institute for Meteorology	0.9375 × 0.9375
29	***MPI-ESM1-2-LR***	Max Planck Institute for Meteorology	1.875 × 1.875
30	***MRI-ESM2-0***	Meteorological Research Institute	1.875 × 1.875
31	***NESM3***	Nanjing University of Information Science and Technology	1.875 × 1.875
32	***NorESM2-LM***	NorESM Climate modeling Consortium	2.5 × 1.875
33	***NorESM2-MM***	NorESM Climate modeling Consortium	1.25 × 0.9375
34	SAM0-UNICON	Seoul National University	1.25 × 0.9375
35	***TaiESM1***	Research Center for Environmental Change	1.25 × 0.9375
36	**ERA5**	European Centre for Medium-Range Weather Forecasts	0.25 × 0.25

Table S1. A list of CMIP6 models and observations considered in this study. The models used for both the HIST and FUT periods are in bold italics.